Cyclic plasticity behaviors of steam turbine rotor subjected to cyclic thermal and mechanical loads

Xuanchen Zhu[1], Haofeng Chen[1,2]*, Fuzhen Xuan[1], Xiaohui Chen[3]

[1] *School of Mechanical and Power Engineering, East China University of Science and Technology, 200237, China*

[2]*Department of Mechanical & Aerospace Engineering, University of Strathclyde, G1 1XJ, UK*

[3] *School of Control Engineering, Northeastern University, Qinhuangdao, 066004, China.*

Abstract

In this paper, shakedown and ratchet analyses are performed to investigate the cyclic plasticity behaviors of the steam turbine rotor subjected to cyclic thermal and mechanical loads by employing Linear Matching Method (LMM). Traditionally, the shakedown or ratchet analysis mainly focus on the structure under general cyclic loading condition composed by constant mechanical load and cyclic thermal load, but the investigated steam turbine rotor here is subjected to cyclic mechanical load and cyclic thermal load that vary in phase and out of phase throughout the practical operation load cycle. The failure behaviours of structure under practical operation load cycle is studied and discussed. The novel shakedown and ratchet failure diagrams are plotted by calculating different combinations of cyclic mechanical load and cyclic thermal load. The innovative equation to acquire plastic strain range of the structure under steady state cycle is fitted, which is vital for low cycle fatigue (LCT) assessment. Moreover, detailed step-by-step inelastic analyses are also performed to verify the applicability and effectiveness of the limit boundaries calculated by the LMM. All the investigations demonstrate that the proposed LMM technique is capable of handling practical industrial application with complicated cyclic loads.

* Corresponding author.
Email: haofeng.chen@strath.ac.uk Tel: +44(0) 141 548 2036

Keywords: Cyclic thermal-mechanical load, Linear Matching Method, Steam turbine rotor, Shakedown failure diagram, Ratchet failure diagram

1 Introduction

The increasing demand for thermal power and environmental restriction on CO_2 emission requires advanced steam turbine with higher efficiency such as ultra-supercritical power units to be applied in coal thermal power plants. The steam turbine rotor, as a core component of steam turbine, subjected to temperature transient and speed variation during repeated start-up, running, shut-down phases that lead the steam turbine rotor to endure cyclic thermal-mechanical load. Hence, the steam turbine rotor may undergo reverse plasticity behaviour or ratchet behaviour, which eventually cut the lifespan of the structure. The shakedown and ratchet limits are therefore necessary to be established for the critical design limits and to show how the structure will fail.

Shakedown and ratchet analyses of the structure/component subjected to cyclic loading have been investigated by many researchers in past decades. The complex nature of the shakedown and ratchetting mechanisms means that analytical solutions are rare to obtain. Therefore, the incremental Finite Element Analysis (FEA) is widely used. In fact, the step-by-step elastic-plastic FEA can only obtain whether the shakedown, reverse plasticity, or ratchetting occurs under the predefined cyclic loading, which requires many repetitive calculations to generate the Bree-like diagram [1]. Consequently, a number of direct methods based on the Koiter's [2] kinematic and the Melan's [3] static theorems have been created to efficiently acquire the shakedown and the ratchet limits. Adibi-Asl and Reinhardt raised a non-cyclic method for shakedown analysis employing a combination of linear and nonlinear FEA [4, 5]. Abdalla et al. proposed a simplified technique to predict the ratcheting boundary of elbow piping [6]. Many other researchers developed a range of mathematical programming methods to calculate the shakedown limit and limit load, including Maier [7], Staat and Heitzer [8], Liu and Carvelli [9], etc. And other methods, including Uniform Modified Yield (UMY) surface method [10], the Generalized Local Stress Strain (GLOSS) r-node method [11], the Reduced Modulus Method [12], the Elastic Compensation Method (ECM) [13, 14], and the Linear Matching Method (LMM) [15-19], were raised for determining limit load, shakedown and ratcheting boundary of

structure components. Among these direct methods, the LMM has been proved to give accurate solutions to practical engineering applications, including structural integrity assessments of superheater outlet penetration tubeplate which involves shakedown and ratchet limit analyses and steady state cyclic analyses [20], lower bound ratchet limit analyses of pipe intersection with dissimilar material join [21-22], etc. The accuracy of LMM has also been proved by experiments recently [23]. The LMM ABAQUS user sub-routines [24] have been consolidated by the R5 [25] research program of British Energy Generation Ltd. (BEGL) to commercial standard, and now in extensive use for the design and/or assessment of power plant components. Other methods either have less ability to analyse complex structure with cyclic load effectively, or difficult to be applied in engineering cases due to the inavailability for convenient programs.

The main goal of this paper is to investigate the failure behaviours of the steam turbine rotor based on practical operation load cycle by using the LMM and then generate the shakedown and ratchet failure diagrams in terms of out-of-phase and in-phase variations between the cyclic mechanical load and cyclic thermal load. In comparison with the most of shakedown or ratcheting applications, where the analysed geometries could almost all be categorized into relatively simple structures such as holed plate, cylinder, straight/elbow pipe, etc. and the loading conditions mainly focus on pure mechanical load or constant mechanical load with cyclic thermal load, this novel irregular structure of shakedown and ratcheting area not only produces more challenges in meshing model and consumes more computational efforts in calculation, but also introduces coupled cyclic thermal-mechanical load into shakedown and ratcheting analyses. Based on it, classic cyclic plasticity failure diagram could be extended into double-cyclic-loads range and it is accessible to assess the novel obtained cyclic plasticity behaviours. The paper is subsequently structured as follows: initially the related formulations behind the LMM are presented in section 2, followed by the description of the geometry model and practical operation load cycle of the steam turbine rotor in section 3, which also presents the temperature and elastic stress field of the structure calculated by the LMM. Shakedown limit analyses (section 4) of the structure under practical operation load cycle are given, then the shakedown limit interaction curves of the steam turbine rotor subjected to cyclic thermal-mechanical load are constructed. ABAQUS step-by-step inelastic analysis is introduced in this part to verify the applicability and effectiveness of the results. In section 5, we fit the equation to calculate the plastic

strain range of the structure under cyclic thermal-mechanical load and also the LMM ratchet limit analyses are carried out to evaluate the capacity of the structure subjected to the existing cyclic thermal-mechanical load to withstand an additional constant mechanical load, where the ratchet limit boundaries of the steam turbine rotor are built up by calculating different combinations of the thermal-mechanical load.

2 Numerical Procedures of the LMM

The material is regarded as isotropic, elastic-perfectly plastic and satisfies the von Mises yield conditions in this section. A typical cycle in the time interval $0 \le t \le \Delta t$ is considered. We consider a structure subjected to a cyclic history of varying temperature $\lambda_\theta \theta(x,t)$ and varying centrifugal force $\lambda_f F(x,t)$ within the volume of the structure and varying surface loads $\lambda_p P(x,t)$ which act over part of the structure's surface S_T. Here, λ denotes a load parameter, allowing a whole class of loading histories to be considered. On the remainder of the surface S, denoted as S_u, the displacement $u = 0$. The corresponding linear-elastic solution history of loading histories is shown as

$$\hat{\sigma}_{ij}(x,t) = \lambda_\theta \hat{\sigma}_{ij}^{\theta}(x,t) + \lambda_f \hat{\sigma}_{ij}^{F}(x,t) + \lambda_P \hat{\sigma}_{ij}^{P}(x,t) \tag{1}$$

where $\hat{\sigma}_{ij}^{\theta}(x,t)$, $\hat{\sigma}_{ij}^{F}(x,t)$ and $\hat{\sigma}_{ij}^{P}(x,t)$ are the elastic solutions caused by $\theta(x,t)$, $F(x,t)$ and $P(x,t)$, respectively.

Then, as a cyclic problem, the stresses and strain rates will become asymptotic to a cyclic state where;

$$\sigma_{ij}(t) = \sigma_{ij}(t + \Delta t), \qquad \dot{\varepsilon}_{ij}(t) = \dot{\varepsilon}_{ij}(t + \Delta t) \tag{2}$$

The cyclic solution is composed of three parts, the elastic solution, a transient solution accumulated up to the beginning of the cycle and a residual solution that on behalf of the remaining changes within the cycle. The cyclic stress history irrespective of material properties is given by

$$\sigma_{ij}(x,t) = \lambda \hat{\sigma}_{ij}(x,t) + \overline{\rho}_{ij}(x) + \rho_{ij}^{r}(x,t) \tag{3}$$

where $\bar{\rho}_{ij}(x)$ denotes a constant residual stress field in equilibrium with zero surface traction on S_T and corresponds to the residual state of stress at the beginning and end of the cycle. The history $\rho_{ij}^r(x,t)$ is the change in residual stress during the cycle which satisfies

$$\rho_{ij}^r(x,0) = \rho_{ij}^r(x,\Delta t) \tag{4}$$

As for the shakedown analysis, this changing constituent part of residual stress $\rho_{ij}^r(x,t) = 0$. Therefore, the cyclic solution for shakedown analysis is shown by

$$\sigma_{ij}(x,t) = \lambda \hat{\sigma}_{ij}(x,t) + \bar{\rho}_{ij}(x) \tag{5}$$

The detailed LMM numerical procedures for shakedown and ratchet analyses were given by Chen [26] based on these steady-state cyclic formulations. For a general cyclic load, it can be disintegrated as cyclic and constant parts, i.e. $\hat{\sigma}_{ij}(x,t) = \hat{\sigma}_{ij}^{\Delta}(x,t) + \lambda \hat{\sigma}_{ij}^{\bar{C}}(x)$. The calculation of shakedown limit only includes conducting a global minimization process to evaluate the constant residual stress caused by the combined action of cyclic and constant loads. The evaluation of ratchet limit contains dual minimization processes: an incremental minimization for the assessment of a cyclic history of changing residual stress caused by predefined cyclic load $\hat{\sigma}_{ij}^{\Delta}(x,t)$ is performed and the corresponding plastic strain range in a steady state cycle is calculated for the LCF purpose at this step. The second step is to conduct a global minimization for ratchet limit caused by an extra constant load, which is as same as the global minimization process to assess constant residual stress of shakedown problems, and however the initial cyclic elastic stress history is augmented by the changing residual stress calculated in the first step.

2.1 Evaluation of upper bound limits

Combining shakedown conditions with a global minimization process of energy, an inequality can be given by

$$I(\Delta\varepsilon_{ij}, \lambda^S) = \int_V \sum_{n=1}^{N} \left\{ \sigma_{ij}^n \Delta\varepsilon_{ij}^n - \lambda^S \hat{\sigma}_{ij}(t_n) \Delta\varepsilon_{ij}^n \right\} dV \geq 0 \tag{6a}$$

$$i.e. \qquad \lambda^S \le \frac{\int_V \left(\sum_{n=1}^{N} \sigma_{ij}^n \Delta\varepsilon_{ij}^n \right) dV}{\int_V \left(\sum_{n=1}^{N} \hat{\sigma}_{ij}(t_n) \Delta\varepsilon_{ij}^n \right) dV} = \frac{\int_V \left(\sigma_y \sum_{n=1}^{N} \bar{\varepsilon}(\Delta\varepsilon_{ij}^n) \right) dV}{\int_V \left(\sum_{n=1}^{N} \hat{\sigma}_{ij}(t_n) \Delta\varepsilon_{ij}^n \right) dV} = \lambda_{UB}^S \tag{6b}$$

where $\Delta\varepsilon_{ij}^n$ is a sequence of increments of strain occurring at a sequence of N times t_n, $n=1$ to N, during the cycle, σ_y is the yield stress of material, and $\bar{\varepsilon}$ denotes the von Mises effective strain. Hence, the upper bound shakedown multiplier λ_{UB}^S can monotonically reduce and converge to the least upper bound limit λ^S of shakedown problem.

For ratchet analysis, an incremental minimization can give the history of the varying residual stress field corresponding to the cyclic part of the load history. Then, Chen et al. [27] has proved that the numerical procedure of ratchet analysis can be adapted to the existing procedure of shakedown analysis where the cyclic linear elastic stress history is augmented by the calculated varying residual stress field, i.e.

$$\hat{\sigma}_{ij} = \lambda \hat{\sigma}_{ij}^{\bar{C}} + \hat{\sigma}_{ij}^{\Delta}(x,t) + \rho_{ij}(x,t) \tag{7}$$

Combining the von Mises yield condition and corresponding flow rule, an upper bound of ratchet limit is then calculated by

$$\lambda_{UB}^R = \frac{\int_V \sum_{n=1}^{N} \sigma_y \bar{\varepsilon}\ (\Delta\varepsilon_{ij}^n) dV - \int_V \sum_{n=1}^{N} (\hat{\sigma}_{ij}^{\Delta}(t_n) + \rho_{ij}(t_n)) \Delta\varepsilon_{ij}^n dV}{\int_V \hat{\sigma}_{ij}^{\bar{C}} \left(\sum_{n=1}^{N} \Delta\varepsilon_{ij}^n \right) dV} \tag{8}$$

Eq. (8) provides the method to calculate the capacity of the structure subjected to a predefined cyclic load to bear an additional constant load before ratchet behavior happens.

2.2 Evaluation of lower bound limits

As described in Melan's lower bound theorem, once the changing residual stress field $\rho_{ij}^r(x,t)$ and the constant residual stress $\bar{\rho}_{ij}(x)$ in Eq.(3) have been calculated by global minimization and incremental minimization processes, we can calculate the lower bound of shakedown or ratchet limit within the upper bound procedure through maximizing the lower bound load parameter λ_{LB} by checking if the steady-state cyclic stresses at all integration points of the body caused by the applied loading history are no more than the yield stress of the material.

Because a sequence of upper bound iterative processes give the residual stress field, we can then scale the elastic solution to calculate the lower bound at each iteration so that the steady-state cyclic stress nowhere violates the yield condition. The lower bound of shakedown limit multiplier is calculated by

$$\lambda_{LB}^{s} = \max\ \lambda_{LB} \tag{9a}$$

$$s.t. \quad f(\lambda_{LB}\hat{\sigma}_{ij}(x,t) + \bar{\rho}_{ij}(x)) \le 0 \tag{9b}$$

The lower bound of ratchet limit multiplier is given by

$$\lambda_{LB}^{R} = \max\ \lambda_{LB} \tag{10a}$$

$$s.t. \quad f(\lambda_{LB}\hat{\sigma}_{ij}^{\bar{F}} + \hat{\sigma}_{ij}^{\Delta}(x,t) + \rho_{ij}(x,t) + \bar{\rho}_{ij}(x)) \le 0 \tag{10b}$$

3 Problem Description and Linear Elastic Solutions

3.1 Geometry and finite element model

The overall view of the rotor is shown in Fig.1 (a). According to the self-characteristic of structure, loading symmetry and the cyclic symmetry condition, 1/91 section of a single rotor wheel is modelled to discuss its failure behaviour under cyclic thermal-mechanical load by using the LMM. Fig.1 (b) exhibits 1/91 rotor wheel with blade root cut from the rotor as there are 91 blades of the whole wheel.

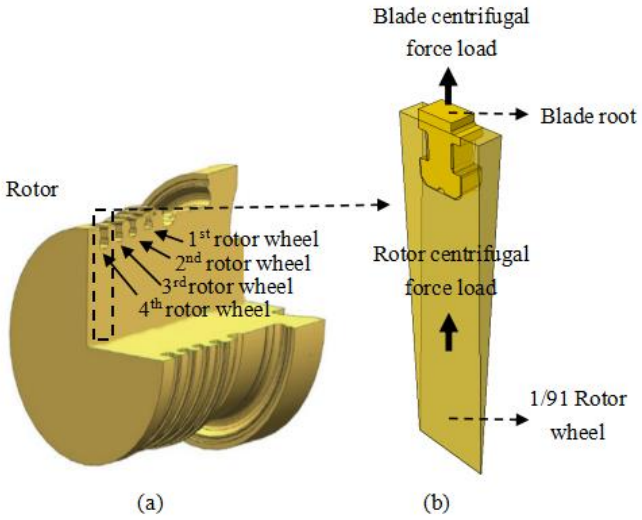

Fig.1. (a) Geometry of the rotor, (b) 1/91 rotor wheel with blade root

The cyclic mechanical load of the structure is caused by the centrifugal force of the blade and the rotor during the repeated start-up, running, shut-down phases. Fig.2(a) shows the mechanical load at the rotor wheel groove, where the cyclic mechanical load is composed of three parts, the load 1 and load 2 represent pressure load caused by blade centrifugal force load which are uniformly acted on the contact surface between the blade root and the rotor wheel groove. The load 1 is bigger than load 2 as the asymmetric design of the blade, and these two loads can be calculated by the rotating speed ω and the area of the contact surface, where the variation of ω is provided in Fig.3. The load 3 is the centrifugal force load of the rotor itself. The rotor gravity is ignored as it is relatively quite small compared with the centrifugal force. Fig.2 (b) displays the thermal-mechanical boundary conditions acting on the 1/91 rotor wheel. The high-temperature steam flow across the rotor surface and the blade root, and significant thermal gradient inside the rotor were caused by the heat-transfer actions which further led to cyclic thermal load with the repeated operations. Fig.2 (c) shows the overall view of the element of the 1/91 rotor wheel with blade root. 9358 elements of 20-node quadratic brick, reduced integration C3D20R were adopted for 1/91 rotor wheel with blade root, 5710 elements of 1/91 rotor wheel and 3648 elements of blade root, respectively.

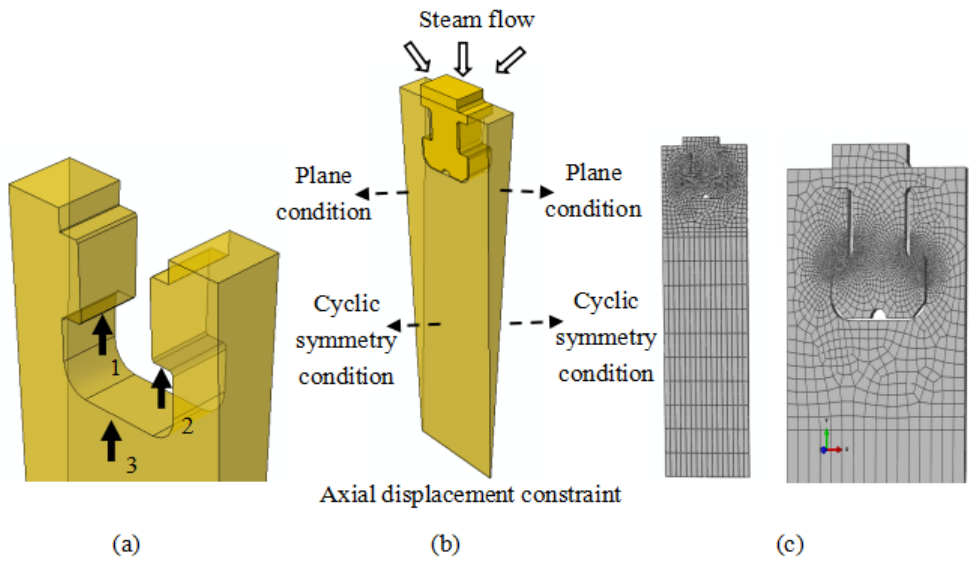

Fig.2. (a) mechanical load of the rotor wheel groove, (b) scheme of thermal-mechanical boundary conditions of 1/91 rotor wheel with blade root, (c) mesh of the 1/91 rotor wheel and blade root

3.2 Material properties and loading conditions

The material of the rotor and the blade root in this paper is the martensitic steels of the 9-12% Cr family. Considering the steam temperatures in recent and projected thermal power stations are now approaching the upper temperature limit for ferritic steels, substantial improvements have been made on 9-12%Cr steels for applying in various steam and gas plants [28], including higher strength, improved oxidation resistance which would reduce the need for cladding, and better resistance to embrittlement during the course of long-term operation at high temperatures. The material properties applied to structural analysis are shown in Table 1. The geometry of the model and operation parameters is provided by the turbine manufacturer.

Table 1 Material properties.

Material property	9-12% Cr
Young's Modulus [GPa]	160
Coefficient of thermal expansion	1.2×10^{-5}
Yield stress [MPa]	240
Poisson's ratio	0.3
Specific heat capacity [J/ kg°C]	460
Thermal conductivity [30 w/m°C]	30
Density [g/cm^3]	7.7

A single practical operation load cycle of steam turbine lasts 2880h (120 days) where the start-up, shut-down phases continue 15h, 96h respectively and the steady running period lasts 2769h. Fig.3 plots the steam temperature and rotating speeds at the main practical operation, where the maximum steam temperature $T_{\max}$ is 600°C and the maximum rotating speed $\omega_{\max}$ equals to 3000r/min. The thermal stress history of the maximum location of the structure is also given in Fig. 3, which is produced by a transient heat-transfer analysis, and a subsequent structural analysis. The LMM selects a finite number of load instants to describe the practical operation load cycle, and other instants with smaller loads are expected to be encompassed. It can be seen that six instants are selected in Fig.3 to construct the cyclic

thermal-mechanical load history, which is submitted to the LMM analysis to stimulate the real repeated start-up, running and shut-down operation of the steam turbine. It is worth noting that the constructed cyclic thermal-mechanical load history had rarely been coupled in the majority of shakedown and ratcheting applications, which makes it accessible to research the novel obtained cyclic plasticity behaviours under this loading cycle. The symbol $\overset{\Delta}{\sigma}_{P\theta 0}$ is applied to denote the practical operation load cycle, which is set as the reference loading history. The descriptions of these six load instants are exhibited in Table 2.

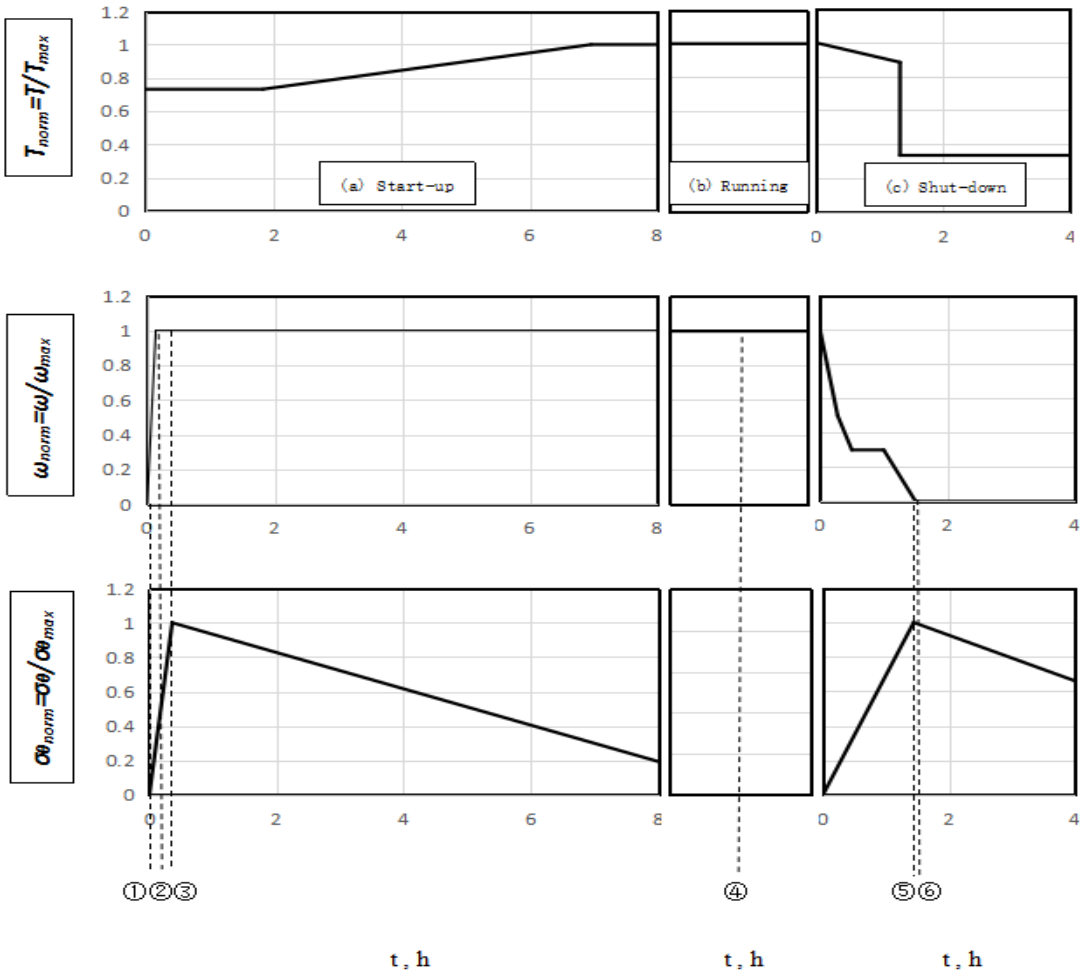

Fig.3. Normalized steam temperature curves, rotating speeds and thermal stress curves of practical operation load cycle for (a) start-up, (b) running, and (c) shut-down phases

Table 2 Six instants selected from steam turbine's practical operation load cycle for submitting in LMM

Instant	①	②	③	④	⑤	⑥
Description	no-working status	the speed reaches rated status of start-up	the most significant thermal stress of start-up	steady operation status	the most significant thermal stress of shut-down	the speed reaches zero of shut-down
Speed (r/min)	0	3000	3000	3000	250.2	0
Temperature (°C)	25	temperature field of this instant	temperature field of this instant	620	temperature field of this instant	temperature field of this instant

3.3 Linear elastic solutions

Temperature and elastic solution data are submitted as input into all LMM analysis, which involve a number of iterative linear analyses to simulate nonlinear plastic material behaviour and represent the history of stress and inelastic strains. Fig.4. gives the contour of von Mises effective elastic stress of the mechanical loads and thermal loads on the six selected instants, respectively. It is worth noting that the mechanical loads of instant ①, ⑥ are zero and instants ②, ③, ④ have similar mechanical load, so only the contour of von Mises effective elastic stress of the mechanical loads of instants ② and ⑤ are shown in Fig. 4. Considering six instants selected for a practical operation load cycle, we denote $\overset{\Delta}{\sigma}_{p0}$ and $\overset{\Delta}{\sigma}_{\theta 0}$ as the linear elastic stress history of the mechanical loads and the thermal loads respectively, i.e. the reference loading history for LMM $\overset{\Delta}{\sigma}_{p\theta 0} = \overset{\Delta}{\sigma}_{p0} + \overset{\Delta}{\sigma}_{\theta 0}$.

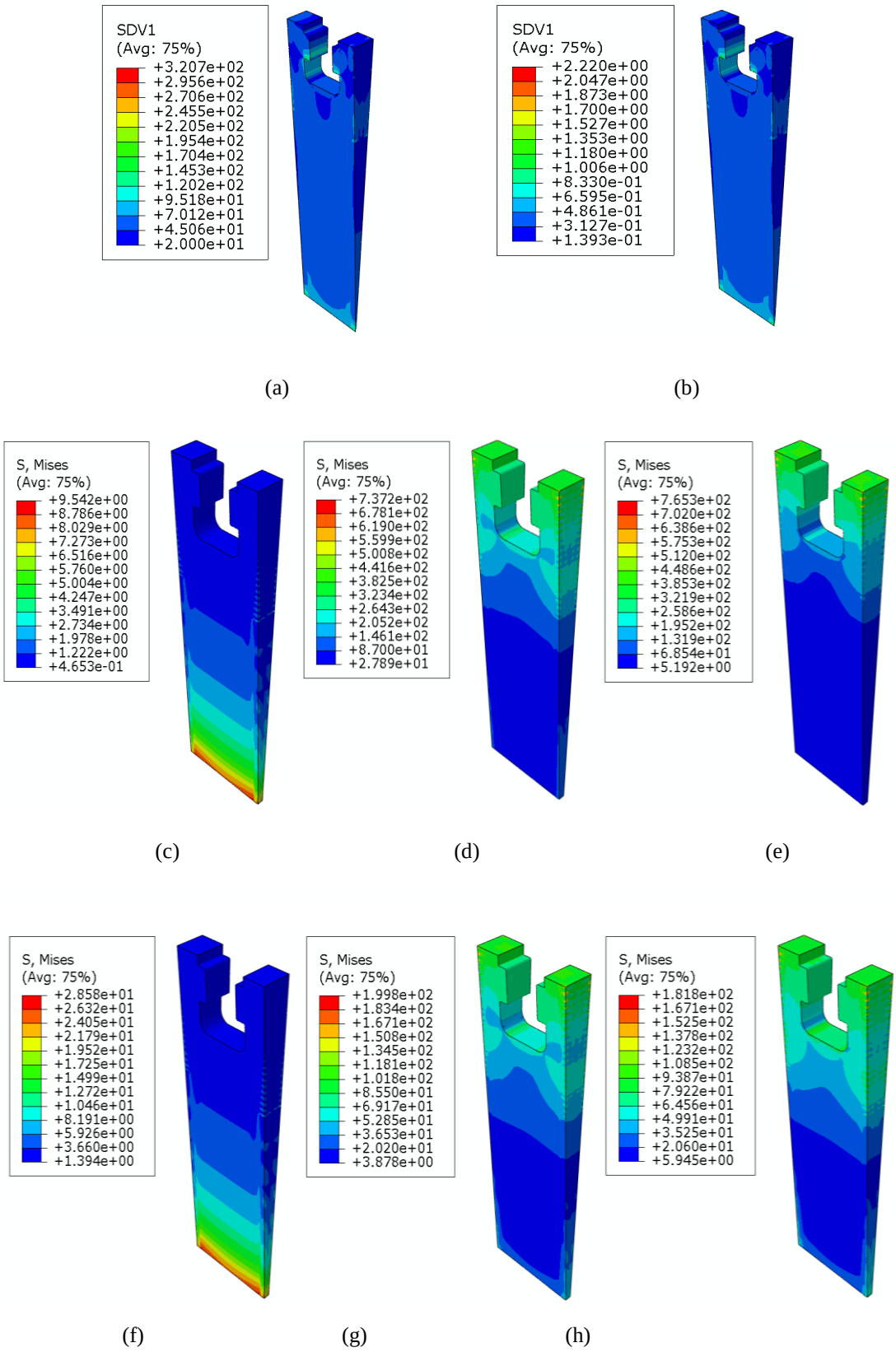

Fig.4. The contour of elastic von Mises effective stress with (a) mechanical load of instant ②, (b) mechanical load of instant ⑤, (c) thermal load of instant ①, (d) thermal load of instant ②, (e) thermal load of instant ③, (f) thermal load of instant ④, (g) thermal load of instant ⑤, (h) thermal load of instant ⑥

The contour of elastic von Mises effective stresses of three composed mechanical loads on instant ② are shown in Fig.5. According to the contours, the self-centrifugal-force has less impact on the significant stress concentration region of the entire body than other two loads, contrary it consumes vast computational efforts. Hence it is of prime importance that we investigate the effect of self-centrifugal-force of steam turbine rotors in structural integrity assessment so as to understand if they have a large impact or if they can be ignored.

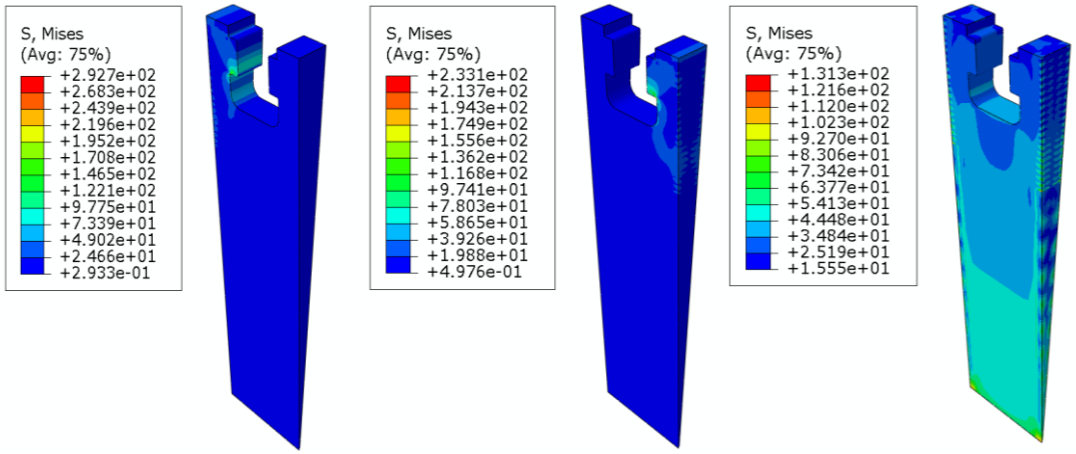

(a) (b) (c)

Fig.5. The contour of elastic von Mises effective stress of three composed mechanical loads on instant ② (a) load 1, (b) load 2, (c) self-centrifugal-force

4 Shakedown Limit Analysis

In terms of the definitions of shakedown limits in LMM (section 2), the shakedown multipliers λ_P^S and λ_θ^S are computed based on the reference loading history to represent the shakedown limits of the structure, i.e. $\lambda_P^S \sigma_{P0}^{\Delta} + \lambda_\theta^S \sigma_{\theta 0}^{\Delta}$, where σ_{p0}^{Δ} and $\sigma_{\theta 0}^{\Delta}$ are the predefined cyclic mechanical load and cyclic thermal load respectively in section 3.3. And ABAQUS step-by-step inelastic analysis is also performed to confirm the accuracy of the computed shakedown limits.

4.1 Shakedown analysis of practical operation load cycle

The shakedown multipliers λ_P^S and λ_θ^S of practical operation load cycle $\sigma_{p0}^{\Delta} + \sigma_{\theta 0}^{\Delta}$ are presented in Table 3. In case 1, with considering the self-centrifugal-force of the rotor, the shakedown limits of

the structure is equal to $0.881\overset{\Delta}{\sigma}_{p0}+0.881\overset{\Delta}{\sigma}_{\theta 0}$, which means the structure under current practical operation load cycle is out of shakedown boundary, and hence further ratchet analysis of this loading history is needed to avoid incremental plastic collapse occurred, and to evaluate the plastic/total strain ranges for the LCF life assessment. Case 2 differentiates with Case 1 as ignoring the effect of self-centrifugal-force of the rotor, and it clearly displays that the difference of shakedown multipliers between these two cases is 1.9%. The calculated converged values of shakedown limits are plotted in Fig.6, where the approximate converged solution can quickly be obtained after 15 iterations and deviation is less than 2% both in Case 1 and Case 2. It is therefore quite feasible for LMM to evaluate shakedown limits with less computational efforts.

Table 3 Shakedown multipliers of steam turbine rotor of practical operation load cycle

	Shakedown multiplier of mechanical load λ_p^S	Shakedown multiplier of thermal load λ_θ^S	self-centrifugal-force
Case 1	0.881	0.881	√
Case 2	0.898	0.898	×

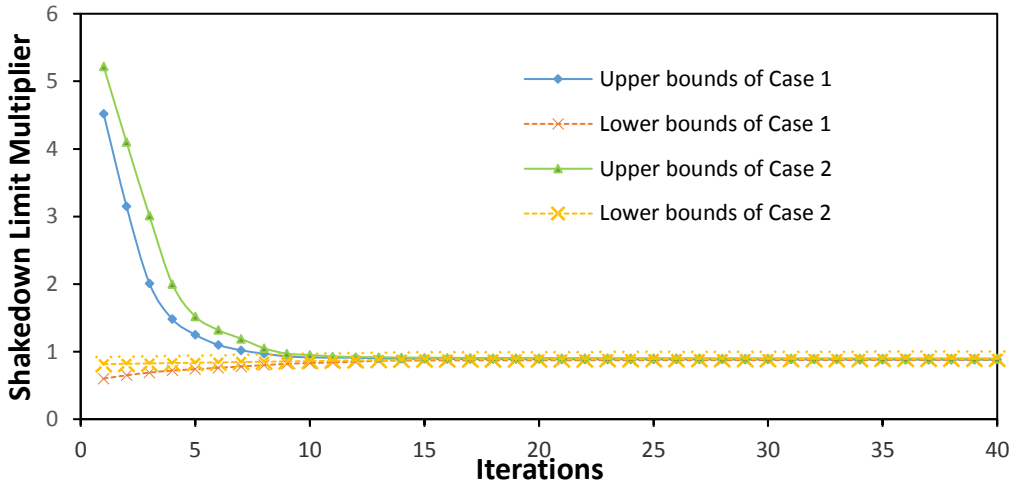

Fig. 6 The convergence condition of iterative processes for shakedown analyses

Fig. 7 plots the contours of overall and maximum location of plastic strain range under steady cyclic

state, where the maximum plastic strain range at the significant mechanical stress concentration region due to cyclic mechanical load component contributes the main parts to the failure mechanism than cyclic thermal load component under current practical operation load cycle. It can also be shown that the plastic strain occurs in a relatively small area and embraced by the elastically responding material around. By comparing the numerical values of maximum plastic strain range between Case 1 and Case 2 from Fig. 7, we can conclude that although the difference of shakedown multipliers is less than 1.9%, there is marked difference in the magnitude of plastic strain range, which is 21.5%. Hence, the self-centrifugal-force of the rotor may not be taken into account for shakedown limit analysis of the similar steam turbine structure, but that is a nonnegligible factor for subsequent low cycle fatigue assessment.

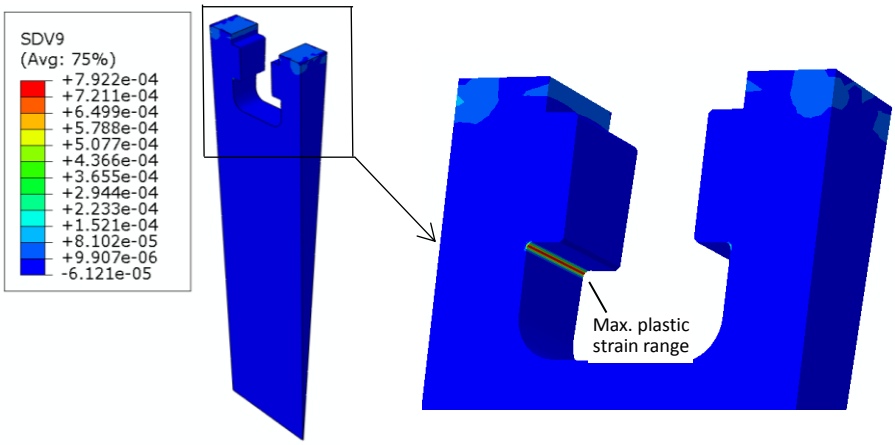

(a)

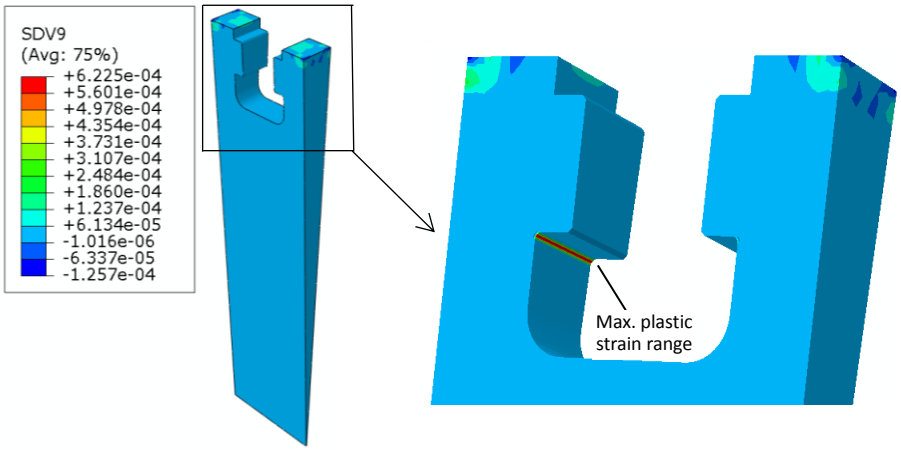

(b)

Fig. 7 Contour plots of overall and maximum location of plastic strain range corresponding to practical operation load cycle (a) Case 1 (b) Case 2

4.2 Shakedown limit interaction curve

By calculating different combinations of cyclic thermal-mechanical load varying in-phase and considering the self-centrifugal-force of the rotor, we plot the shakedown limit interaction curves of the steam turbine rotor subjected to an arbitrary cyclic thermal-mechanical load (Fig. 8). In Fig.8, the non-dimensional value of X-coordinate represents the ratio of the applied cyclic mechanical stress with the reference cyclic mechanical stress, where $\frac{\overset{\Delta}{\sigma}_p}{\overset{\Delta}{\sigma}_{p0}}=1$ corresponds to the current practical operation mechanical load. The non-dimensional value of Y-coordinate means the ratio of the applied cyclic thermal stress with the reference cyclic thermal stress, where $\frac{\overset{\Delta}{\sigma}_\theta}{\overset{\Delta}{\sigma}_{\theta 0}}=1$ represents the current practical operation thermal load. *R* in legend represents the angle between load history and X-axis.

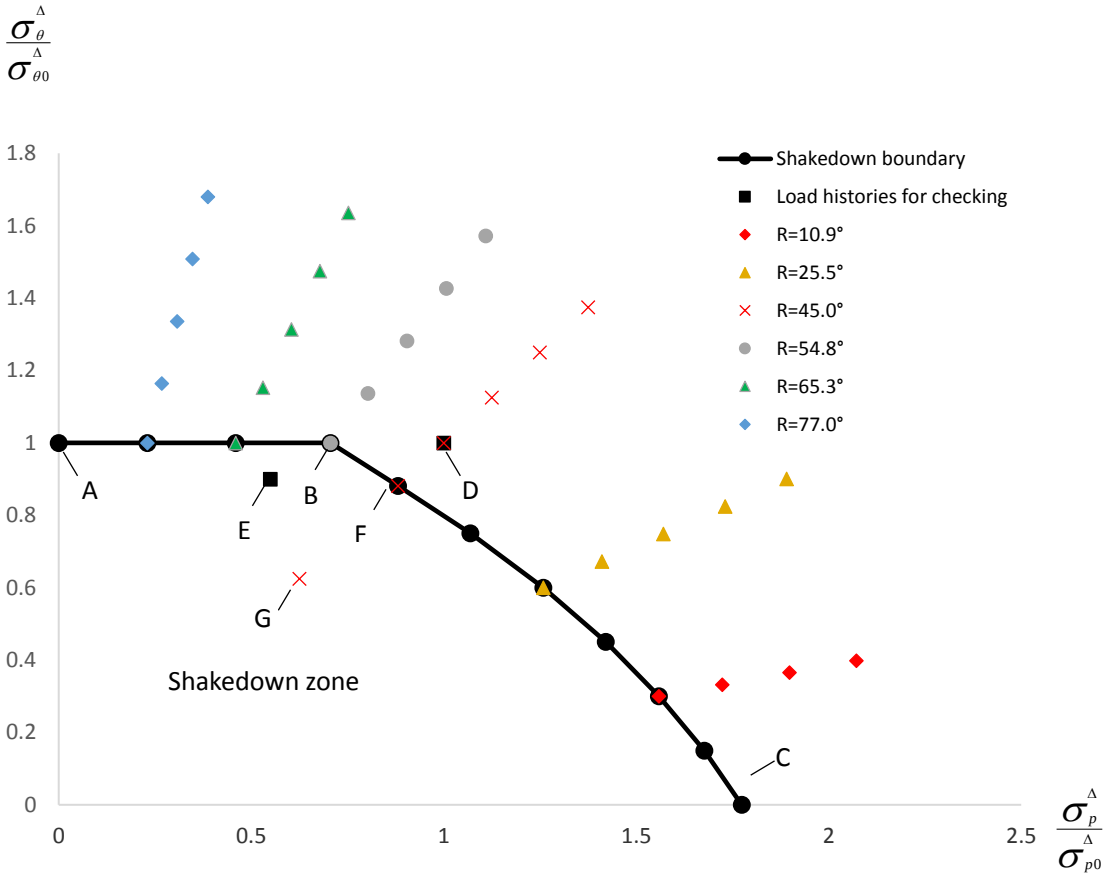

Fig. 8 The shakedown limit interaction curves of the steam turbine rotor subjected to cyclic thermal-mechanical load

As given in Fig. 8, the entire loading histories can be divided into two regions, where the elastic shakedown occurs within the region of ABC. The current practical operation load cycle, which is

denoted as point D in Fig. 8, lies outside the shakedown limit boundary, and in order to determine whether the load point is in reverse plasticity region or ratchet region, further ratchet limit analysis is needed to be taken. It is also worth noting that the point C corresponds to the shakedown limit of the applied cyclic mechanical loads, which is $1.774\sigma_{p0}^{\Delta}$. It is a coincidence that the obtained shakedown limit of the applied cyclic thermal loads is the practical operation cyclic thermal load $\sigma_{\theta 0}^{\Delta}$, which is represented as Point A in Fig. 8. In comparison with the classic Bree-like diagram, which leaves marginal failure features of the structure under constant mechanical load and cyclic thermal load, these shakedown limit interaction curves extend the classic cyclic plasticity failure diagram into the range of coupled cyclic thermal-mechanical load. In other words, cyclic plasticity behaviors under coupled cyclic thermal-mechanical load are innovatively incorporated into safety margins assessment.

4.3 ABAQUS step-by-step inelastic analysis

ABAQUS step-by-step inelastic analysis is applied to verify the applicability and effectiveness of shakedown limit computed by the LMM. Loading history within the shakedown limits boundary (Point E in Fig.8) and practical operation load cycle (Point D in Fig.8) which is out of shakedown limit boundary are selected to observe its plastic strain history at the peak location of the structure. As is shown in Fig.9 (a), which is the history of plastic strain magnitude of Point E within 20 load cycles, inelastic plastic strain occurs at the early cycles, and then the subsequent cycles show no more new plastic strain, which indicates an elastic shakedown status of the structure. It can also been seen that the practical operation load cycle of the structure leads to an alternating plasticity mechanism as shown in Fig.9 (b), where the positive plastic strain equals to the negative plastic strain during the cycle and net growth of plastic strain (i.e. ratchetting) will not occur. These steady cycles of plastic strains exhibit that the practical load operation of the structure is out of elastic shakedown region and enters the reverse plasticity, i.e. global shakedown region. Hence the ratchet limit analysis may be carried out to search the margin of this particular loading history to the ratchet limit boundary.

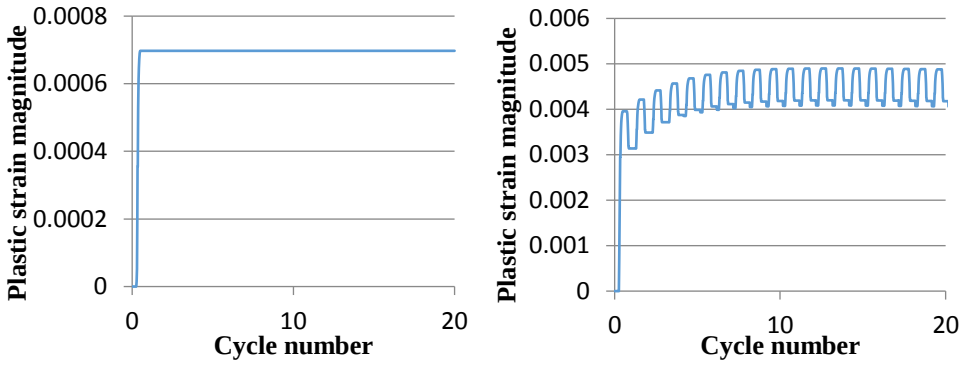

Fig. 9 Plastic strain history of peak location of the steam turbine rotor: (a) Point E under 20 cycles and (b) Point D under 20 cycles

Hence, the accuracy of the shakedown limit boundaries computed by LMM has been demonstrated by ABAQUS step-by-step inelastic analyses. Meanwhile, by comparing the computational efforts involved in the LMM and ABAQUS step-by-step method, a conclusion can be drawn that the usage of LMM is much cheaper than the step-by-step method, especially for the cyclic load histories, as the LMM can directly give the shakedown limit with one single calculation.

5 Steady State Cycle and Ratchet Limit Analysis

If the applied cyclic loading is out of elastic shakedown limit boundary, either the reverse plasticity or ratcheting mechanism will happen. The low cycle fatigue mechanism empirically occurs at the area of localised reverse plasticity and the maximum plastic strain range may determine the number of cycles to failure. The ratchetting behaviour which eventually leads to an incremental plastic collapse must be avoided. The LMM is capable of providing not only the steady cyclic state solutions involving both residual stress field and plastic strain ranges during the cycle but also the ratchet limit with a sufficient accuracy.

5.1 Steady cyclic state

Fig. 8 shows six angles of load histories, along which the cyclic thermal-mechanical loads vary in-phase based on the reference loading history. We plot the maximum plastic strain of the structure under these loading histories in Fig. 10, where the X-axis denotes the ratio between the distance of the load history from origin and the distance of shakedown limit point along the angle from the origin in Fig, 8. D_e is introduced on behalf of the ratio and $D_e = 1$ in the X-axis represent the shakedown

limit boundary point of the structure, where the theoretical plastic strain range is zero.

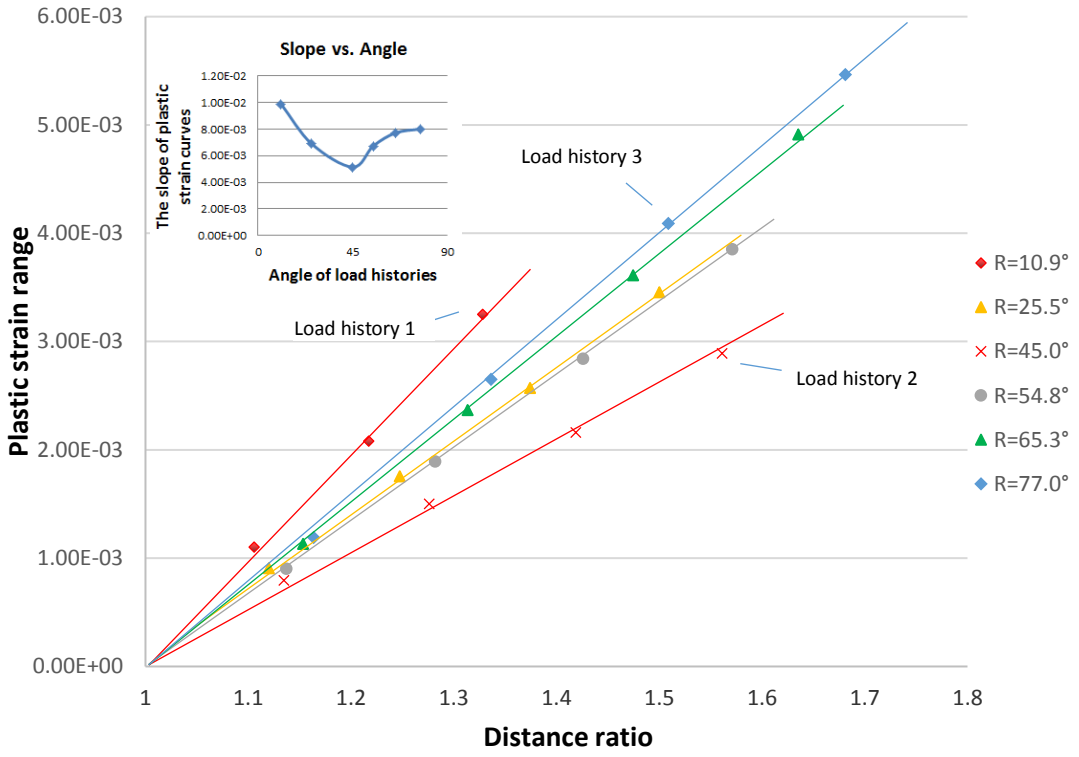

Fig. 10 The plastic strain range of the structure subjected to load histories along six angles

As reported in Fig. 10, there is a linear distribution of the plastic strain range along these angles. Then, we give the curve of the slope vs. the angle, in which the entire angle range is divided into two parts by 45°. For the region within 45°, the plastic strain range is mainly dominated by the cyclic mechanical load, and Fig. 11 (a) shows the plastic strain range of load history 1 (R=10.9°, Fig. 10) where the primary plastic strain occurs at the acting region of the cyclic mechanical load. Whereas for the region out of 45°, the cyclic thermal load is the primary effective load. The significant plastic strain of load history 3 (R=77.0°, Fig. 10) occurs at the region where the cyclic thermal load applied as shown in Fig. 11 (c). Hence the following equations can be fitted to acquire the maximum plastic strain range of the structure under cyclic thermal-mechanical load which varies corresponding to reference loading history.

$$\Delta\varepsilon_p = \left[-0.003\ln(R) + 0.0179\right]D_e \qquad (R \le 45°) \qquad (11a)$$

$$\Delta\varepsilon_p = \left[-0.0032R^2 + 0.4819R - 10.011\right]D_e \qquad (R \ge 45°) \qquad (11b)$$

where the plastic strain range is determined by R that is the angle of load history with origin of coordinates in Fig. 8 and non-dimensional ratio of distance D_e. In this paper, we creatively connect the plastic strain range with the location of the loading history in plasticity failure diagram and then innovatively fit equations for calculating plastic strain range. From that, plastic strain range can conveniently be acquired by identifying the location of the loading history in shakedown failure diagram and submitted to the further low cycle fatigue assessment. It is worth noting that the plastic strain range is produced by novel coupled cyclic thermal-mechanical load, which has rarely been estimated before.

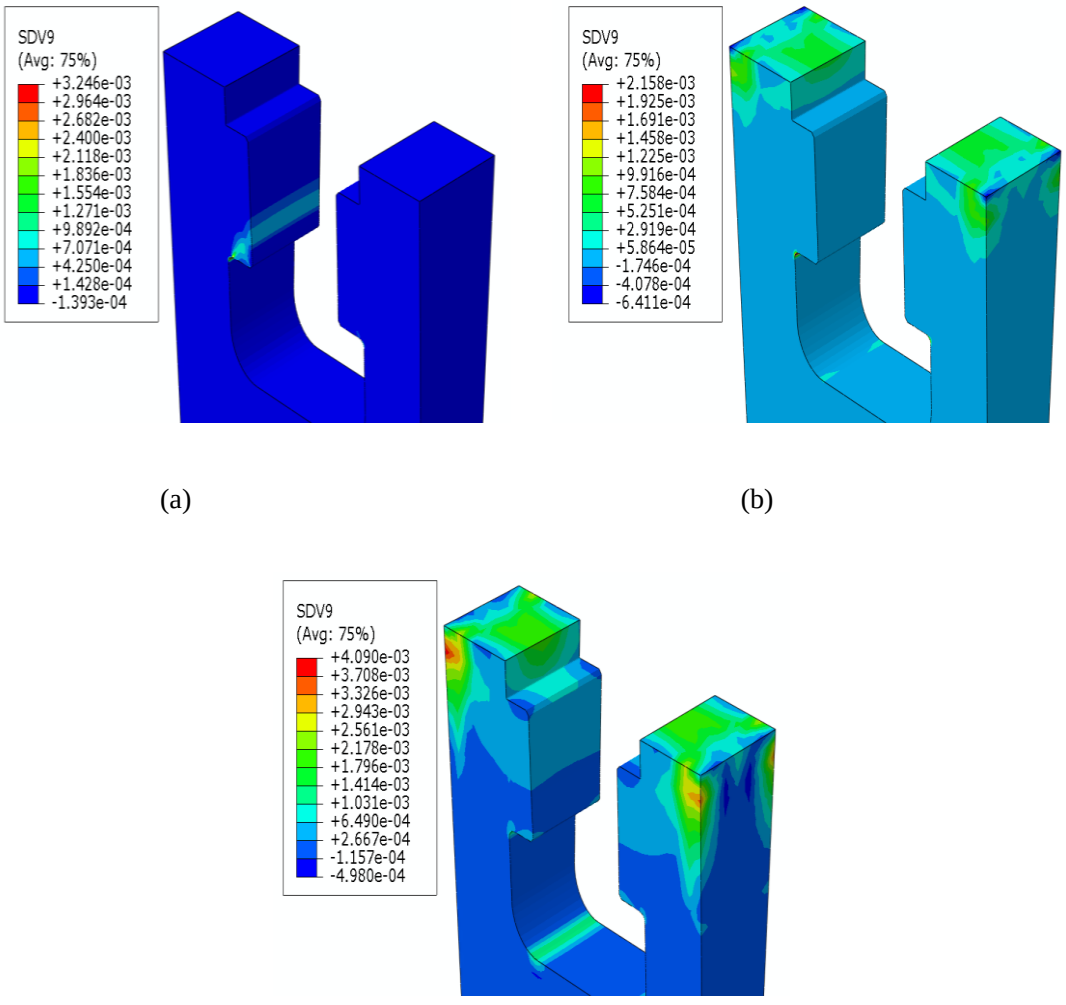

(a) (b)

(c)

Fig. 11 The contour of plastic strain range of the structure under (a) load history 1 (R=10.9°), (b) load history 2 (R=45.0°) and (c) load history 3 (R=77.0°)

5.2 Ratchet analysis of practical operation load cycle

The numerical procedure of obtaining ratchet limit (section 2) provides the method to calculate the capacity of the structure subjected to a predefined cyclic load to accommodate an additional constant load before ratchet behavior happens. Hence, the ratchet limit of the structure is given by $\lambda_{\Delta}^{R}\sigma_{P\theta 0}^{\Delta}+\lambda_{C}^{R}\sigma_{P0}$ where σ_{P0} is an additional constant mechanical reference load that is equal to the mechanical load at the running phase in magnitude, which is the maximum mechanical load of the whole start-running-shut process and set as reference constant mechanical load in this section. λ_{Δ}^{R} and λ_{C}^{R} denote the ratchet limit multipliers of the predefined reference loading history $\sigma_{P\theta 0}^{\Delta}$ and reference additional load σ_{P0}.

In terms of shakedown limit analysis in section 4, we can only see that the structure under current practical operation load cycle is experiencing reverse plastic behaviour. Hence the ratchet limit analysis is needed to discuss how close the applied loading history is to the ratchet limits boundary. Table 4 exhibits two ratchet limit assessments of practical operation load cycle. As is shown in Case 1, $\sigma_{P\theta 0}^{\Delta}+1.057\sigma_{P0}$ is the ratchet limit of the structure under practical operation status, which means the current cyclic loading history plus 1.057 times the reference constant mechanical load will reach the ratchet boundary of the structure. The difference between Case 1 and Case 2 lies on whether the effect of self-centrifugal-force is included. By comparing the results of these two cases, we can conclude that the self-centrifugal-force contributes only less than 2.1% to the ratchet limit multiplier of practical operation load cycle, therefore this load is a subordinate load for the designing of the ratchet limit of the structure.

Table 4 Ratchet limit multipliers of steam turbine rotor subjected to practical operation load cycle

	Ratchet multiplier of reference loading history λ_{Δ}^{R}	Ratchet multiplier of constant load λ_{C}^{R}	self-centrifugal-force
Case 1	1	1.057	√
Case 2	1	1.079	×

5.3 Ratchet limit interaction curve

We calculate different combinations of cyclic thermal-mechanical load and constant mechanical load, then plot the shakedown and ratchet limit interaction curves in Fig. 12. The arbitrary applied constant mechanical load is normalized with respect to the reference constant mechanical load σ_{P0} in the X-axis and the applied cyclic thermal-mechanical load in the Y-axis is normalized by reference cyclic load $\sigma_{P\theta 0}^{\Delta}$ which is denoted as point D as practical operation load cycle. The practical operation status is in reverse plasticity zone as reported in Fig. 9b, where the LMM produces not only the same results but also consumes much less computational efforts comparing with the ABAQUS full inelastic analysis. It is also worth noting that the point C on the X-axis of Fig. 12 represents the limit load of the applied constant mechanical load, however the point C in Fig. 8 is the shakedown limit of the applied cyclic mechanical load.

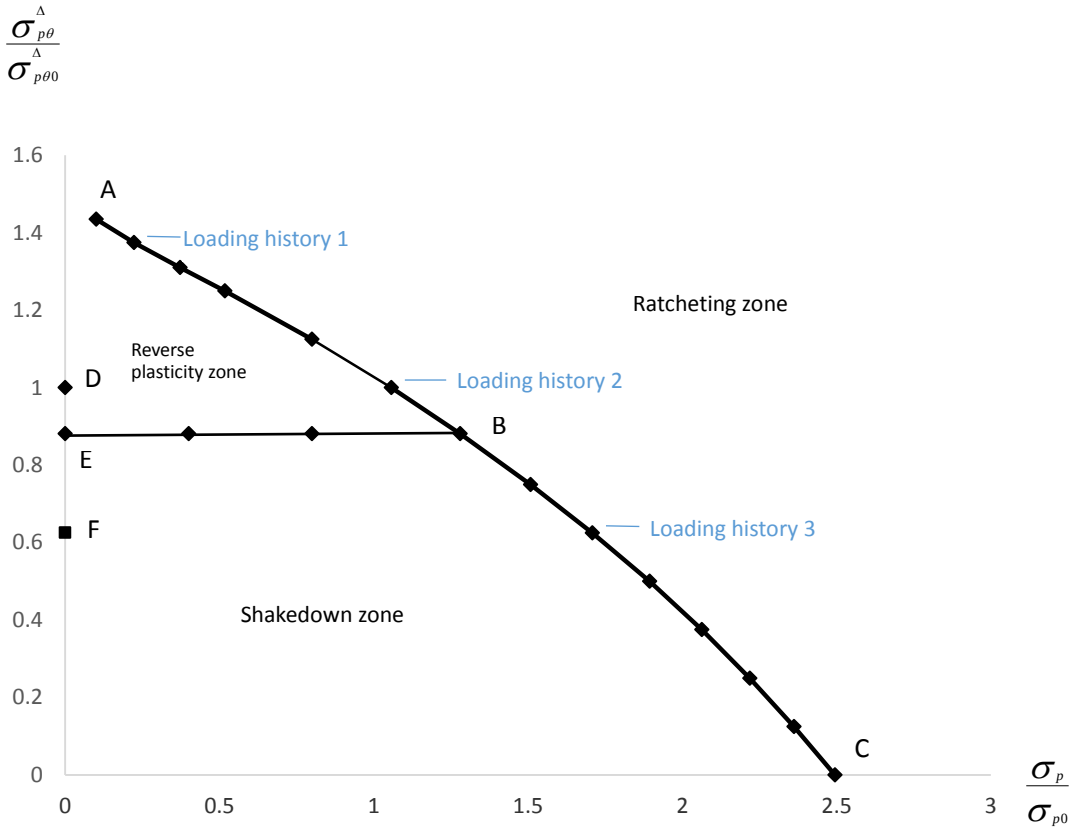

Fig. 12 The shakedown and ratchet limit interaction curves of the steam turbine rotor subjected to cyclic thermal-mechanical load

As is shown in Fig. 12, the limit boundaries divide the entire loading zone into three regions. If the applied load within the shakedown limit EBC, a certain amount of plastic strain may build up during the first few cycles, after that the structure behaves elastically again. When the loading histories locate in reverse plasticity zone ABE, the plastic strain during the cycle alternates in compression and tension and they are equal in magnitude, which is also known as “alternating plasticity”. If the applied load is beyond the ratchet limit boundary ABC, either the incremental plastic collapse will happen where the plastic strain accumulates during each cycle or the plastic collapse occurs immediately after the loading if the ratchet limit is identical to the limit load of the structure. The ratchet strain distributions of three loading histories (load point 1, 2 and 3 shown in Fig. 12) are given in Fig. 13, where the ratchetting behaviours of these three loading histories are similar and all the failures occur on the most significant acting region of mechanical load even for greater cyclic thermal-mechanical loading history (Load point 1) and follow 45° around cut off along the force direction, which means the failure mechanism of ratchetting behaviour for current structure mainly dominated by the additional mechanical loading

regardless of how big the predefined cyclic thermal-mechanical loading is.

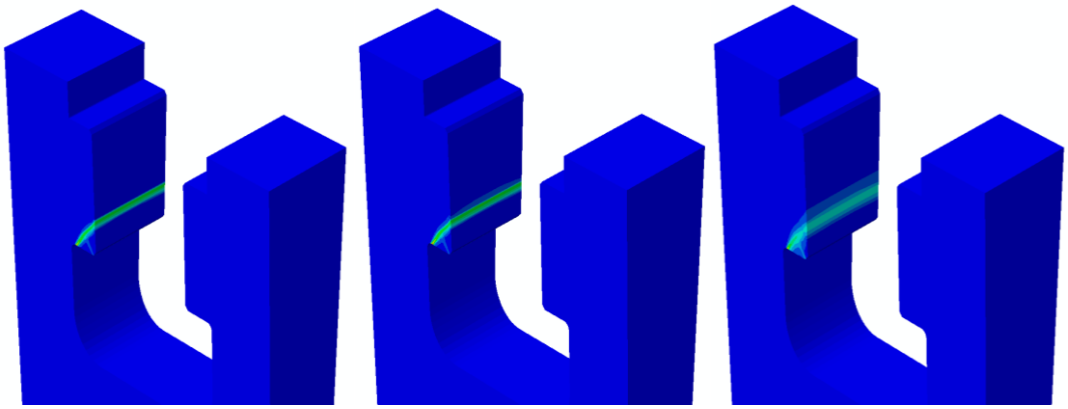

(a) (b) (c)

Fig. 13 Contour plots of maximum location of ratchet strain magnitude corresponding to loading histories (a) Load history 1 (b) Load history 2 (c) Load history 3

Fig. 12 denotes the shakedown limit as the capacity of the structure subjected to a predefined cyclic thermal-mechanical load to accommodate an additional constant mechanical load, where the applied cyclic thermal-mechanical load vary strictly in-phase based upon the predefined load cycle. While the shakedown limit given in previous shakedown analysis (Fig. 8) is the limit of the structure subjected to cyclic thermal-mechanical load that vary out-of-phase throughout the respective reference loading history. Considering the loading history of Point G in Fig. 8 for example, which is the same loading condition as Point F of Fig. 12, the obtained results in Fig. 8 show that how many amplification times of cyclic mechanical component or cyclic thermal component of this loading history will trigger the non-shakedown behaviours of the structure. Fig. 12 gives the shakedown limits as the capacity for the structure subjected to this loading history to accommodate the amount of an additional constant mechanical reference load σ_{p0}. Hence, the LMM provides the efficient method to calculate shakedown, ratchet limit of the structure with respect to in-phase and out-of-phase variations between the cyclic mechanical and thermal loads.

6 Conclusions

This paper casts light on the cyclic plasticity behaviors of the steam turbine rotor subjected to

complex cyclic thermal-mechanical load by using the LMM, where the load histories vary in phase and out of phase throughout the practical operation load cycle. The structure under current practical operation load cycle is investigated, and the results display that this load history is out of elastic shakedown region and enters reverse plasticity zone. Plastic strain range is synchronously given for possible low cycle fatigue assessment, from which it can be observed that the plastic strains occur in a relatively small range at mechanical stresses concentration region and embraced by the elastically responding material around. Self-centrifugal-force of the rotor has been proved to affect the shakedown and ratchet limits of the structure to a limited extent, as 1.9% and 2.1% respectively. Conversely the plastic strain is observably influenced as 21.5%. For further designing of the same structure, self-centrifugal-force should be allocated different concerns depend on the type of analysis.

The shakedown boundaries calculated by the LMM are plotted in two ways, one is the limits of the structure to accommodate out of phase varying cyclic thermal-mechanical load and the other one is the capacity of the steam turbine rotor subjected to in phase varying practical operation load cycle to withstand an additional constant load. A Bree-like diagram with ratchet limit boundaries is also given, by replacing the cyclic thermal load with the cyclic thermal-mechanical load. These integrated cyclic plasticity failure diagrams are further used to study the interaction between the different failure mechanisms and to avoid the reduction of structure life. By calculating cyclic thermal-mechanical loads that vary in phase along six angles, equations have been fitted to acquire plastic strain ranges of the steam turbine rotor under cyclic thermal-mechanical loads depending on practical operation load cycle. The equations are divided into two components due to an arbitrary load history, which is either dominated by cyclic mechanical load or cyclic thermal load. The plastic stain range can then easily be obtained by identifying the location of the targeted load history in obtained shakedown failure diagram.

A number of ABAQUS step-by-step inelastic analyses are also performed for the validation purposes. All the results demonstrate that the LMM is capable of simulating a wider range of loading circumstances including out-of-phase and in-phase variations between the cyclic mechanical and thermal loads, and providing accurate shakedown and ratchet limit boundaries, with high computational efficiency.

Acknowledgements

The authors gratefully acknowledge the support of East China University of Science and Technology and the University of Strathclyde during the course of this work.

References

[1] Bree, J., 1989. Plastic deformation of a closed tube due to interaction of pressure stresses and cyclic thermal stresses. International Journal of Mechanical Sciences, 31 (11-12) (1989), pp. 865-892.

[2] Koiter, W.T., 1960. General theorems for elastic plastic solids. J.N. Sneddon, R. Hill (Eds.), Progress in solid mechanics, North Holland, Amsterdam (1960), pp. 167-221.

[3] Melan, E., 1936. Theorie statisch unbestimmter Systeme aus ideal-plastichem Baustoff. Sitzungsber. d. Akad. d. Wiss., Wien, 2A(145) (1936), pp. 195–218.

[4] Adibi-Asl, R, Reinhardt, W., 2011. Non-cyclic shakedown /ratchetting boundary determination – part 1: analytical approach. International Journal of Pressure Vessels and Piping, 88 (8-9) (2011), pp. 311-320.

[5] Adibi-Asl, R, Reinhardt, W., 2011. Non-cyclic shakedown /ratchetting boundary determination – part 2: numerical implementation. International Journal of Pressure Vessels and Piping, 88 (8-9) (2011), pp. 321-329.

[6] Abdalla, HF, Megahed MM, Younan, MYA, 2011. A simplified technique for shakedown limit load determination of a large square plate with a small central hole under cyclic biaxial loading. Nuclear Engineering and Design, 241 (3) (2011), pp. 657-665.

[7] Maier, G., 1977. Mathematical programming methods for deformation analysis at plastic collapse. Computers and Structures, 7, pp. 599-612.

[8] Staat, M., Heitzer, M., 2001. LISA a European Project for FEM-based Limit and Shakedown Analysis. Nuclear Engineering and Design, 201, pp. 151-166.

[9] Liu Y.H., Carvelli V., Maier G., 1997. Integrity assessment of defective pressurized pipelines by

direct simplified methods. International Journal of Pressure Vessels and Piping, 74, pp. 49-57.

[10] Abou-Hanna, J., McGreevy, T.E., 2011. A simplified ratchetting limit method based on limit analysis using modified yield surface. International Journal of Pressure Vessels and Piping, 88 (1) (2011), pp.11-18.

[11] Seshadri, R., 1995. Inelastic evaluation of mechanical and structural components using the generalized local stress strain method of analysis. Nuclear Engineering and Design, 153 (2-3) (1995), pp. 287-303.

[12] Marriott, D.L., 1998. Evaluation of deformation or load control of stresses under inelastic condition using elastic finite element stress analysis. ASME Pressure Vessel and Piping conference, Pittsburg, PA, pp. 3-9.

[13] Mackenzie, D., Boyle, J.T., Hamilton, R., Shi, J., 1996. Elastic compensation method in shell-based design by analysis. Proceedings of the 1996 ASME Pressure Vessels and Piping Conference, 338 (1996), pp. 203-208.

[14] Mackenzie, D., Boyle, J.T., Hamilton, R., 2000. The elastic compensation method for limit and shakedown analysis: a review. Trans IMechE, Journal of Strain Analysis for Engineering Design, 35 (3) (2000), pp. 171-188.

[15] Ponter, A.R.S., Carter, K.F., 1997. Limit state solutions, based upon linear elastic solutions with a spatially varying elastic modulus. Computer Method in Applied Mechanics and Engineering, 140 (3-4) (1997), pp. 237-258.

[16] Ponter, A.R.S., Carter, K.F., 1997. Shakedown state simulation techniques based on linear elastic solutions. Computer Methods in Applied Mechanics and Engineering, 140 (3-4) (1997), pp. 259-279.

[17] Ponter, A.R.S., Fuschi, P., Engelhardt, M., 2000. Limit analysis for a general class of yield conditions. European Journal of Mechanics - A/Solids, 19 (3) (2000), pp. 401-421.

[18] Ponter, A.R.S., Engelhardt, M., 2000. Shakedown limits for a general yield condition: implementation and application for a Von Mises yield condition. European Journal of Mechanics - A/Solids, 19 (3) (2000), pp. 423-445.

[19] Engelhardt, M., 1999. Computational modelling of Shakedown. PhD thesis, University of Leicester.

[20] Chen, H.F., Ponter, A.R.S., 2009. Structural integrity assessment of superheater outlet penetration tubeplate. International Journal of Pressure Vessels and Piping, 86 (7) (2009), pp. 412-419.

[21] Chen, H.F., Ure, J., Tipping, D., 2013. Calculation of a lower bound ratchet limit part 1 – Theory, numerical implementation and verification. European Journal of Mechanics - A/Solids, 37 (2013), pp. 361-368.

[22] Ure, J., Chen, H.F., Tipping, D., 2013. Calculation of a lower bound ratchet limit part 2 – Application to a pipe intersection with dissimilar material join. European Journal of Mechanics - A/Solids, 37 (2013), pp. 369-378.

[23] Ure, J., Chen, H.F., Tipping, D.J., 2015. Verification of the Linear Matching Method for limit and shakedown analysis by ccomparison with experiments. Journal of Pressure Vessel Technology, Transactions of the ASME, 137 (3) (2015), pp. 031003-1 - 031003-6.

[24] Tipping, D.J., 2007. The Linear Matching Method: A Guide to the ABAQUS User Subroutines. E/REP/BBGB/0017/GEN/07, British Energy Generation.

[25] Ainsworth, R.A. (editor), 2003. R5: Assessment Procedure for the High Temperature Response of Structures, 3, British Energy Generation Ltd.

[26] Chen, H.F., 2010. Linear matching method for design limits in plasticity. Computers, Materials and Continua – Tech Science Press, 20 (2) (2010), pp. 159-183.

[27] Chen, H.F., Ponter A.R.S., 2010. A direct method on the evaluation of ratchet limit. Journal of Pressure Vessel Technology, 132 (4) (2010), pp. 041202.

[28] Ulrich, E.Klotz, 2008. Martensitic–austenitic 9–12% Cr steels—Alloy design, microstructural stability and mechanical properties. Materials Science and Engineering: A, 476, pp 186-194